A Three-Dimensional Model for the Hammerhead Ribozyme Based on Fluorescence Measurements

Thomas Tuschl, Christoph Gohlke, Thomas M. Jovin, Eric Westhof, Fritz Eckstein*

For the understanding of the catalytic function of the RNA hammerhead ribozyme, a three-dimensional model is essential but neither a crystal nor a solution structure has been available. Fluorescence resonance energy transfer (FRET) was used to study the structure of the ribozyme in solution in order to establish the relative spatial orientation of the three constituent Watson-Crick base-paired helical segments. Synthetic constructs were labeled with the fluorescence donor (5-carboxyfluorescein) and acceptor (5-carboxytetramethylrhodamine) located at the ends of the strands constituting the ribozyme molecule. The acceptor helix in helix pairs I and III and in II and III was varied in length from 5 to 11 and 5 to 9 base pairs, respectively, and the FRET efficiencies were determined and correlated with a reference set of labeled RNA duplexes. The FRET efficiencies were predicted on the basis of vector algebra analysis, as a function of the relative helical orientations in the ribozyme constructs, and compared with experimental values. The data were consistent with a Y-shaped arrangement of the ribozyme with helices I and II in close proximity and helix III pointing away. These orientational constraints were used for molecular modeling of a three-dimensional structure of the complete ribozyme.

The hammerhead ribozyme is an RNA structure that promotes a magnesium ion–dependent site specific cleavage of RNA either in an inter- or an intramolecular reaction (*1*). The latter has attracted particular attention inasmuch as it opens the possibility for inhibition of gene expression by cleavage of the corresponding mRNA (*2*). The secondary structure of the hammerhead ribozyme (Fig. 1) was originally derived from phylogenetic comparison (*3*) and later was supported by thermodynamic nearest-neighbor calculations (*4*, *5*). Probing of the hammerhead ribozyme with ribonucleases confirmed the predicted base-paired structure (*6*). Nuclear magnetic resonance spectroscopy studies have also established the presence of the three double-stranded regions but so far have not provided further insight into the overall structure of the ribozyme (*7*). Initial x-ray diffraction studies of a *trans* acting ribozyme-inhibitor complex and of an inactivated self-cleaving hammerhead domain have been reported (*8*). Here we describe the determination of the relative spatial arrangements of the three helices in the hammerhead ribozyme substrate complex by fluorescence resonance energy transfer (FRET). This method has been successfully applied to investigate structural features of nucleic acids (*9*, *10*), in particular for the determination of the arrangements of the DNA helical arms in the Holliday junction (*11*).

The application of FRET requires the attachment of a fluorescent donor molecule (D) and an acceptor molecule (A) to the nucleic acid under study. In many previous FRET studies with oligodeoxynucleotides the fluorescent acceptor and donor were attached to separate strands at the 3' or 5' ends, respectively, but simultaneous attachment to the same strand has not been reported. This strategy offers a significant advantage in that an excess of unlabeled complementary strand can be used to ensure the rapid and complete binding of the fluorescently labeled strand. This condition is essential for the characterization of ribozymes for which the dissociation constants for short RNA substrates are of the order of a 100 to 1000 nM (*12*, *13*). We therefore adopted this labeling procedure (Fig. 2). Because fluorescence is very sensitive to the molecular environment of the dye, the sequences of the 3 terminal base pairs (bp) were kept unchanged. Likewise the linker used to attach the isomerically pure dyes was kept the same throughout the synthesis of the different oligoribonucleotide constructs (*14*). Cleavage of the substrate was prevented by the incorporation of a single 2'-deoxycytidine at the cleavage site. The FRET efficiencies of RNA duplexes 9 to 18 bp in length (*15*) were measured and interpreted on the basis of the known helical geometry of A-RNA, as described for DNA (*10*, *16*–*18*).

The prediction of FRET efficiency for kinked helices requires information about the localization of the dyes relative to the RNA helix. The positions of the donor and acceptor dyes are given in terms of parameters specifying their relative localization (d, a, L, Δ) (Fig. 3) and must be consistent with the maximum linker length and the anisotropic properties of the dyes. The high anisotropy of 5-carboxytetramethylrhodamine (*17*) indicates the existence of a strong interaction of this dye with the conjugated RNA, presumably through a contact of its positively charged dimethylamino groups with a phosphate group upstream of its 3' attachment site. In contrast, the low anisotropy of 5-carboxyfluorescein (*17*) is indicative of high rotational freedom, suggesting a maximal extension of the linker resulting in minimization of dye-RNA contacts, possibly as a consequence of electrostatic repulsion between the negatively charged 5-carboxyfluorescein and the phosphates. This consideration leads to a localization of 5-carboxyfluorescein above the major groove of the 5' labeled base pair. Using cylindrical polar coordinates (r, θ, z) specified by Arnott for A-RNA atoms (*19*), we located 5-carboxyfluorescein at (d, $-29.5°$, L, -3.75 Å) and 5-carboxytetramethylrhodamine at (a, $-29.5°$; Δ, -3.75 Å) in the case of attachment to the same phosphate ($N = 1$). Within the described constraints, the polar angles θ could not be smaller but might still be as much as 40° larger, and the localization of the dyes along the z axis could vary by ± 5 Å. The angular variation of the dye position affects notably the predicted FRET efficiency for kinked

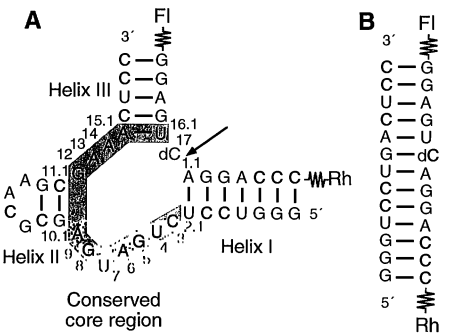

Fig. 1. Sequence and secondary structure of a fluorescein labeled hammerhead ribozyme (**A**) and a continuous double helix (**B**). Nucleotides that are essential for cleavage activity are shaded in gray. The numbering for the hammerhead is according to Hertel *et al.* (*26*). Arrow, usual cleavage site. The donor molecule, 5-carboxyfluorescein (Fl), was linked to the 5' end of the substrate strand while the corresponding acceptor dye, 5-carboxytetramethylrhodamine (Rh), was attached to the 3' end. Unlabeled complementary oligoribonucleotide or ribozyme could be hybridized to the fluorescent strand to form either the control A-RNA duplex or the ribozyme-substrate complex.

T. Tuschl and F. Eckstein, Max-Planck-Institut für Experimentelle Medizin, Hermann-Rein-Str. 3, D-37075 Göttingen, Germany.
C. Gohlke, Abteilung für Molekulare Biologie, Institut für Molekulare Biotechnologie e. V., D-07745 Jena, Germany.
T. M. Jovin, Max-Planck-Institut für Biophysikalische Chemie, Am Faßberg, D-37077 Göttingen, Germany.
E. Westhof, Institut de Biologie Moléculaire et Cellulaire du CNRS, F-67084 Strasbourg, France.
*To whom correspondence should be addressed.

helices, whereas variation along the helix axis causes only relatively minor effects. A systematic variation of these parameters for the prediction of the relative orientations of the ribozyme helices and the evaluation of potential dye RNA contacts led to the use of the proposed dye positions.

The relative spatial orientation of two helices can be described with a minimum of three translational (x, y, z) and three rotational (ϕ, θ, ψ) parameters, the rotational parameters being defined according to the x-convention for Euler angles (*20*). Thus, the helix arrangement of the ribozyme is defined by two sets of six parameters.

Two different series of ribozyme constructs (Fig. 2, A and B) (*21*) were synthesized to derive the orientation $(x, y, z, \phi, \theta, \psi)^{III-I}$ of helix I relative to helix III and the orientation $(x, y, z, \phi, \theta, \psi)^{II-III}$ of helix III relative to helix II. Each member of a given series differed in the number of base pairs within the acceptor helix so that the acceptor dye was moved in the defined geometry of the A-RNA along the acceptor stem. FRET efficiencies were measured for each of these constructs (Fig. 4).

For the determination of the relative helix orientation, it was preferable to simulate a kink in a continuous A-helix by a $(x, y, z, \phi, \theta, \psi)$-coordinate transformation and to compare calculated and measured FRET efficiencies. The transformed helix was chosen to be the acceptor helix, whereas the donor helix remained untransformed. The expected FRET efficiencies for various lengths of the acceptor helix were calculated from Eq. 2 (*17*) as a function of $(x, y, z, \phi, \theta, \psi)$. All orientation parameters were varied systematically, and the calculated FRET efficiencies were compared with the experimental values. Transformation sets that described the relative orientation of helices III to I and II to III within the experimental error were selected. The parameters $(x, y, z, \phi, \theta, \psi)$ specify the transformation in a right-handed Cartesian coordinate system that has the origin at a given phosphorus atom in the labeled strand of a continuous A-form double helix. In this coordinate system, the z axis runs parallel to the helix axis, pointing in the 5' direction of the fluorescently labeled strand. The x axis points radially outward from the helix axis.

It is important to ensure a constant environment of the dyes in the different ribozyme constructs. Interactions of a helix or the core of the ribozyme with the fluorescent dye might also occur, such that the calibration curve of FRET efficiency (Fig. 4) might no longer be valid. Such contacts are registered by unexpected changes of the anisotropies of the dyes. Interference of stem loop II with the acceptor dye in substrates SA11 to SA14 occurred when the stem loop was 4 base pairs (bp) in length. When this stem loop II was shortened to 2 bp, only the acceptor dye in SA11 was affected by the proximity of the helix. Changes in helix II from 4 to 2 bp do not affect the catalytic properties of the ribozyme (*22*), and conformational changes are therefore unlikely. An additional interference at the acceptor dye in construct RD20 was observed. For these reasons, we did not restrict the transformation parameters to a single set but rather considered a family of possible orientation parameters.

Ribozyme structures were calculated by two subsequent coordinate transformations for any combination of the selected orientation parameters. Helix III was generated by the coordinate transformation $(x, y, z, \phi, \theta, \psi)^{II-III}$ of a continuous helix in orientation of helix II at a site equivalent to the 5' phosphorus of A14. Helix I was obtained by a $(x, y, z, \phi, \theta, \psi)^{III-I}$ transformation of the continuous helix III at the site corresponding to the 5' phosphorus of C17 (Fig. 5A). Transformation sets that reflected accurate transfer from helix I to II were selected. Those resulting in van der Waals clashes of the helices were eliminated. Two classes of potential ribozyme structures became evident (Fig. 5B) and could be described by

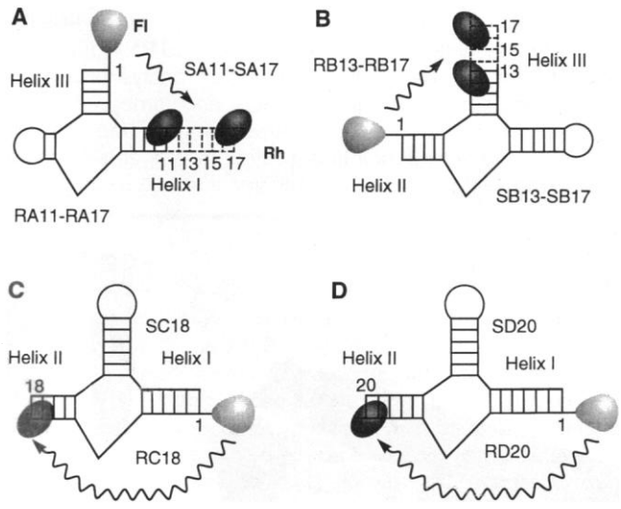

Fig. 2. Outline of the secondary structure of the different hammerhead ribozyme-substrate constructs in the FRET study. FRET is represented by an arrow from the donor 5-carboxyfluorescein (bright sphere) to the acceptor 5-carboxytetramethylrhodamine (dark sphere). The strong interaction of 5-carboxytetramethylrhodamine with the 3' terminal base pairs and the free rotatability of 5-carboxyfluorescein at the 5' end are symbolized. Donor and acceptor helices are varied in a systematic manner. Acceptor walking experiments were performed to measure the relative orientation of the three helices. Constructs of type A were used to determine the relative orientation of helix I with respect to helix III. The length of the acceptor helix I was varied from 5 to 11 bp corresponding to a separation of the donor from the acceptor dye of 11 to 17 nt. Constructs of type B defined the relative orientation of helix III with respect to helix II. Donor and acceptor were separated by 13 to 17 nt. Constructs C and D represent single experiments to measure the distance between the dyes that are linked to helix I and II. Construct D differed from C by the insertion of one additional base pair in each of the donor and the acceptor helices (*21*). Nucleotide numbering indicates the number of nucleotides separating the donor from the acceptor.

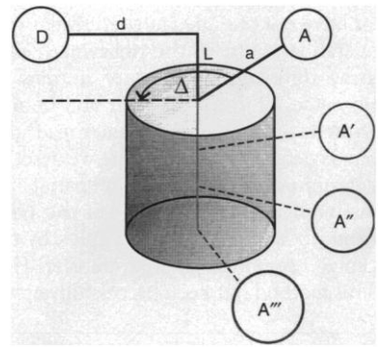

Fig. 3. An A-RNA helix as a cylinder with N base pairs to illustrate the parameters that describe the relative positions of donor (D) to acceptor dye (A). Definitions: d and a, distances of D and A from the cylinder axis, respectively; L and Δ, axial and azimuthal displacement between D and A for the dyes attached to the same phosphate atom ($N = 1$). Primed acceptor symbols illustrate the walking of the dye when attached to successive base pairs. The experimental FRET efficiencies E of continuous A-RNA double helices were represented by the following equation

$$E = \left\{1 + \left[\frac{(2.81\text{Å} \cdot (N-1)+L)^2 + a^2 + d^2 - 2 \cdot a \cdot d \cdot \cos(32.7° \cdot (N-1) + \Delta]^{1/2}}{R_0}\right]^6\right\}^{-1} \quad (1)$$

with $a = 15.80$ Å, $d = 13.87$ Å, $L = 13.32$ Å, and $\Delta = -138.5°$. Each base pair increases the helix length by 2.81 Å (helical rise) with a helical twist of 32.7° (*19*). R_0 was given the value of 43 Å from the measured spectral overlap integral calculated according to (*27*), and an assumed orientation factor κ^2 of 2/3. The parameters d, a, L and Δ were selected for optimal agreement with the central region ($N = 12$ to 16) of the RNA duplex FRET data which must be regarded as provisional, pending further investigation until orientation effects are available and FRET efficiency based on both donor quenching and acceptor sensitization can be precisely evaluated.

either a Y-shape or an h-shape. The latter class directs the seven-nucleotide (nt) conserved loop between helix I and II away from the core and leaves the cleavage site isolated. This structural class was ignored because it would not explain the strict sequence and functional group requirements for ribozyme cleavage. In contrast, the Y-shaped class directs the 7-nt loop through the core and allows contacts to the cleavage site. Within this class, a structure was selected whereby the distance x between the 5'-phosphorus and the 3'-phosphorus atom of cytidine (C17) at the cleavage site was $5 < x < 8$Å, and the separation of the 3'-oxygen atoms of U2.1 of helix I and U16.1 of helix III was >16Å. The selected orientations are suitable for modeling of the core structure and the cleavage site (Fig. 6). The h- and Y-shaped structures differ significantly from those proposed by Mei *et al.* (*23*), which were based on computational studies, and by Gast *et al.* (*24*), which was based on electrophoretic and hydrodynamic methods.

In the Y-shaped arrangement of the helices, helix III forms the apex and helices I and II the two arms. The closest phosphorus-phosphorus distances between helix I and II are within 10 to 15 Å. The calculated orientation of the three helices was used as a starting point for modeling the core structure, consisting of the 7-nt and 3-nt conserved single-stranded stretches, in order to check whether such an arrangement could lead to a plausible geometry at the cleavage site. The FRET results do not provide direct information on the arrangement of nucleotides in this region. For the modeling, we optimized stacking between bases and maintained right-handed paths for the polynucleotide chain. Geometrical and stereochemical knowledge was imposed by the restraint least-squares refinement programs NUCLIN-NUCLSQ (*25*). The 3-nt stretch 5'-GAA leaves helix II and joins helix III following a right-handed path. The 7-nt stretch 5'-CUGAUGA winds its way between the three helices forming the central core. The last 5 nt follow a right-handed path almost in continuity with the 5' strand of helix II. A sharp turn was built after the first 2 nt of that loop, departing from helical continuity with helix I. With this choice, residue G5 is at the same level as the first base pair of helix III (A15.1 · U16.1) in the deep groove side and could possibly form a triple interaction with A15.1 via its N2 amino group. A6 stacks between A15.1 and A14, whereas A9 is in position to form a pair with G12. The cytosine base at the

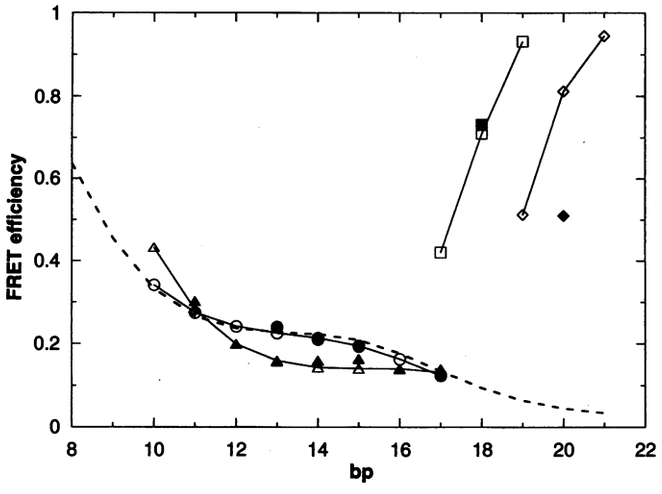

Fig. 4. Dependence of FRET efficiencies on the number of base pairs separating the donor and acceptor dye of the ribozyme constructs of type A (△), B (○), C (□), and D (◇) (Fig. 2). Full symbols indicate experimental values. Open symbols represent calculated values for the three ribozyme helices with relative spatial orientation (4 Å, 4 Å, 0 Å, −10°, −40°, 80°)$^{II-III}$ and (3 Å, 9 Å, 0 Å, −80°, −30°, 130°)$^{III-I}$. For comparison, the transfer efficiencies of the continuous A-RNA double helix (Eq. 1) is given by the dashed line. Helices I and II show transfer efficiencies relative to helix III comparable to the values of the extended continuous double helices, whereas the high FRET signals from helix I to II indicate the close proximity of these two helices. The acceptor dye anisotropies for SA11 and RD20 were decreased from 0.31 to 0.27, indicating that the molecular environment of the acceptor is changed presumably by the close proximity of helices I and II.

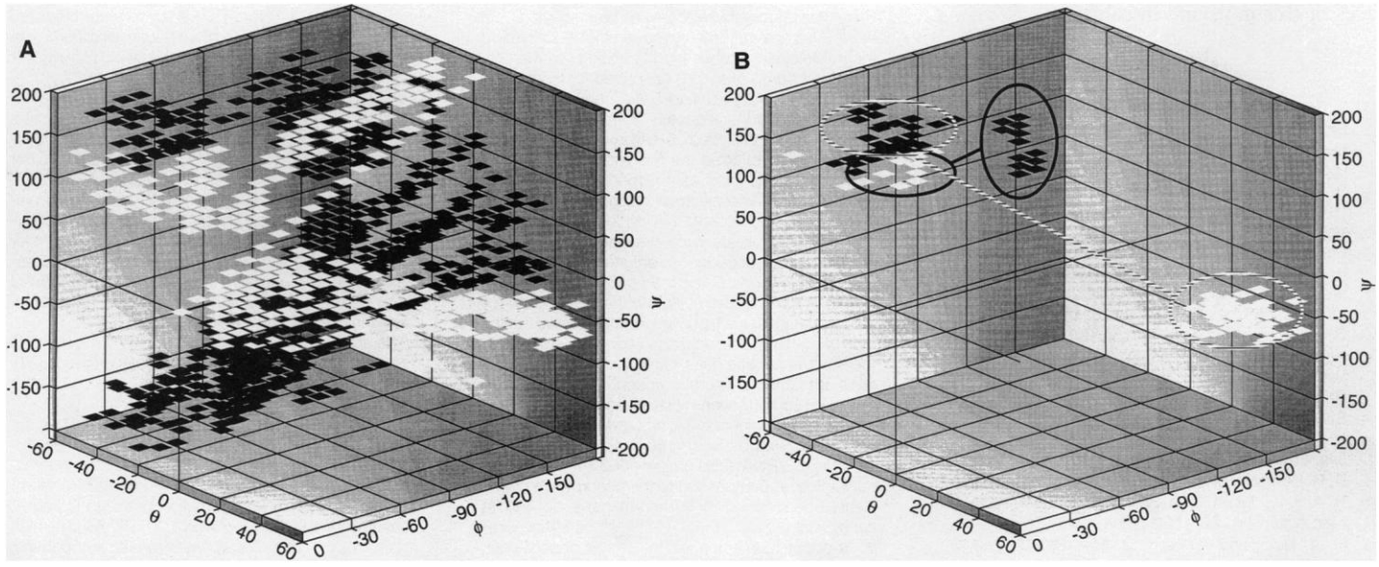

Fig. 5. (**A**) Euler angle space (ϕ, θ, ψ) describing the orientation of helix III relative to helix I (constructs of type A, ■) and helix III relative to helix II (constructs of type B, □) within the experimental error of FRET measurements. Translation parameters (x, y, z) were systematically varied up to ±10 Å (not shown). (**B**) Selected transformation parameters that are consistent with FRET measurements from helix I to II (constructs C and D) followed by the exclusion of van der Waals clashes of helices. Data points in the connected circled regions represent two classes of transformation parameters that describe the relative orientation of all three helices. The class representing an h-shaped structure (broken line) was rejected from model building. A member of the class of Y-shaped structures (closed line) was selected for the structural model in Fig. 6.

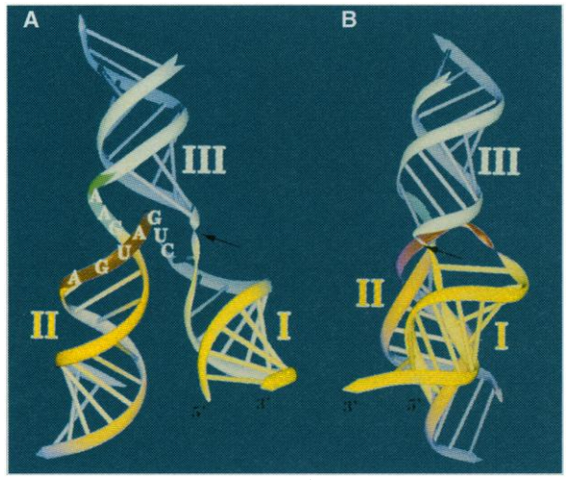

Fig. 6. Ribbon model of two orientations of the Y-shaped helix arrangement of the hammerhead ribozyme. Each helix is represented by a full 11-bp turn. The pathway of the 3-nt and 7-nt conserved loop is modeled into the ribozyme core to be consistent with the orientation of the three helices. Invariant nucleotides in the core are indicated by letters; a) frontal view; b) side view turned left by 90°; arrow, clevage site. Drawing made with the program DRAWNA (*28*) on a Silicon Graphics Extreme 2 Indigo graphics station.

cleavage site points toward the backbone between G5 and A6. The 2′-hydroxyl group of G5 could participate in a potential magnesium binding site together with the hydroxyl of C17 at the cleavage site, one anionic phosphate oxygen of A6 and the O4 or N3 base atoms of U4. Thus, the choice for the paths of the two conserved stretches is characterized, beyond some possible tertiary base-base H-bond interactions, by interdigitation of the bases with potential contacts with sugar-phosphate backbone atoms. A more detailed description of this region of the hammerhead is not justified on the basis of the FRET results.

In summary, we present FRET data on constructs of the hammerhead ribozyme leading to the determination of the spatial arrangement of the three Watson-Crick helices of this molecule in solution.

REFERENCES AND NOTES

1. J. Bratty, P. Chartrand, G. Ferbeyre, R. Cedergren, *Biochim. Biophys. Acta* **1216**, 345 (1993); D. M. Long and O. C. Uhlenbeck, *FASEB J.* **7**, 25 (1993); R. H. Symons, *Annu. Rev. Biochem.* **61**, 641 (1992).
2. S. Altman, *Proc. Natl. Acad. Sci. U.S.A.* **90**, 10898 (1993); O. C. Uhlenbeck, in *Antisense Research and Application*, S. T. Crooke and B. Lebleu, Eds. (CRC Press, Ann Arbor, MI 1993), pp. 83–96; P. Marschall, J. B. Thomson, F. Eckstein, *Cell. Mol. Neurobiol.* in press; J. J. Rossi, D. Elkins, J. A. Zaia, S. Sullivan, *AIDS Res. Human Retroviruses* **8**, 183 (1992).
3. G. Bruening, *Methods Enzymol.* **180**, 546 (1989); P. Keese and R. H. Symons, in *Viroids and Viroid-Like Pathogens*, J. S. Semancik, Ed. (CRC Press, Boca Raton, FL, 1987), pp. 1–47.
4. S. M. Freier *et al.*, *Proc. Natl. Acad. Sci. U.S.A.* **83**, 9373 (1986); J. A. Jaeger, D. H. Turner, M. Zuker, *ibid.* **86**, 7706 (1989).
5. R. B. Denman, *BioTechniques* **15**, 1090 (1993).
6. R. A. J. Hodgson, N. J. Shirley, R. H. Symons, *Nucleic Acids Res.* **22**, 1620 (1994).
7. H. A. Heus and A. Pardi, *J. Mol. Biol.* **217**, 113 (1991).
8. H. W. Pley, D. S. Lindes, C. Deluca-Flaherty, D. B. McKay, *J. Biol. Chem.* **268**, 19656 (1993); R. Kim *et al.*, *Acta Crystallogr.* **D50**, 290 (1994).
9. R. A. Cardullo, S. Agrawal, C. Flores, P. C. Zamecnik, D. E. Wolf, *Proc. Natl. Acad. Sci. U.S.A.* **85**, 4846 (1988); H. Ozaki and L. W. McLaughlin, *Nucleic Acids Res.* **20**, 5205 (1992); L. E. Morrison and L. M. Stols, *Biochemistry* **32**, 3095 (1993); J.-L. Mergny *et al.*, *Nucleic Acids Res.* **22**, 920 (1994); S. Sixou *et al.*, *ibid.*, p. 662; K. Rippe, V. Dötsch, T. M. Jovin, in *DNA, Interaction with Ligands and Proteins. Problems of Recognition and Self-Organization. Fundamental Aspects and Technical Trends*, T. Funck, Ed. (Nova Science, Commarck, NY, in press).
10. R. M. Clegg, A. I. H. Murchie, A. Zechel, D. M. J. Lilley, *Proc. Natl. Acad. Sci. U.S.A.* **90**, 2994 (1993); C. Gohlke, A. I. H. Murchie, D. M. J. Lilley, R. M. Clegg, *ibid.*, in press.
11. A. I. H. Murchie *et al.*, *Nature* **341**, 763 (1989); R. M. Clegg *et al.*, *Biochemistry* **31**, 4846 (1992).
12. M. J. Fedor and O. C. Uhlenbeck, *Biochemistry* **31**, 12042 (1992).
13. D.-J. Fu, S. B. Rajur, L. W. McLaughlin, *ibid.* **32**, 10629 (1993).
14. Oligoribonucleotides were prepared by automated chemical synthesis as described (*29*). Fluorescein labels were introduced by coupling of a 5-carboxyfluorescein phosphoramidite (FAM) (Applied Biosystems Inc.) (*30*). An amino group attached to a 7-carbon linker was introduced by performing the oligoribonucleotide synthesis on 3′-amino modifier C7 CPG (Glen Research). Subsequent conjugation with 5-carboxytetramethylrhodamine was carried out with 5-carboxytetramethylrhodamine succinimidyl ester (Molecular Probes Inc.) in analogy to the procedure of Aurup *et al.* (*31*) described for isothiocyanate coupling to yield 1 to 5 A_{260} units of double-labeled oligoribonucleotides. To remove traces of noncovalently attached 5-carboxytetramethylrhodamine, we hybridized the fluorescent strands to a slight excess of their complementary targets and purifed by native gel electrophoresis (*31*). Only single bands of the fluorescent RNA duplexes or ribozyme-substrate complexes were present, indicating that no alternative secondary structures for these constructs were formed. The ratio of 5-carboxyfluorescein to 5-carboxytetramethylrhodamine absorbance was constant for all purified complexes while the ratio of dye to nucleic acid absorbance decreased as the number of base pairs increased, an indication of constant labeling. The absorption coefficients (ε) in duplexed conformation in 50 mM sodium cacodylate (pH 7.5) were ε(fluorescein) (490 nm) = 22,000 M^{-1} cm^{-1} and ε(rhodamine) (560 nm) = 51,000 M^{-1} cm^{-1} with ε(RNA) (260 nm) = 6600 M^{-1} cm^{-1} per nucleotide. In comparison to the absorbance coefficients of the free dyes, ε(rhodamine) is not significantly affected by conjugation, whereas ε(fluorescein) is about four times lower. Similar observations have been reported (*11*). Absorbance melting curves of the labeled oligoribonucleotide duplex SA13 · C13 (*15*) and of ribozyme substrate complexes SA13 · RA13 and SA17 · RA17 (*21*) were recorded at 10 mM $MgCl_2$, 50 mM sodium cacodylate (pH 7.5) at strand concentrations of 2 μM. A hyperchromicity at 490 nm of about 30% for 5-carboxyfluorescein and a hypochromicity at 260 nm of about 10% for 5-carboxytetramethylrhodamine was observed upon melting of the strands. For ribozyme-substrate complexes, melting of the 5-carboxyfluorescein labeled arm was independently monitored from the melting of the 5-carboxytetramethylrhodamine labeled arm. In the 13-nt-long ribozyme-substrate complex (5 bp at helix I, 7 bp at helix III) both helices melted at about 60°C, whereas for the 17-nt-long complex (5 bp at helix I, 11 bp at helix III) helix I melted at 65°C and helix III at 75°C. The melting temperature of the continuous 13 bp double helix was 85°C. Cleavage kinetics for construct A type ribozyme-substrate complexes are well documented (*12, 22, 32*). Those of the type C and D have also been reported (*13*) as have those of type B (*34*). Fluorescent labeling did not affect ribozyme cleavage. This was confirmed for the ribozyme-substrate construct RA13 · SA13-riboC where the cleavage under multiple turnover condition was followed by the disappearance of the FRET signal. It was also confirmed for construct C where k_{obs} = 0.25 min^{-1} at 1.3 μM substrate was found at 55°C in agreement with reported values (*13*).
15. Oligoribonucleotides used to measure FRET of the continous RNA double helix: Sequences for complementary strands are not given. They did not contain deoxyribose substitutions; C13, complementary to SA13.

    H9, 5′-Fl-GGA GAG CCC-Rh; H10, 5′-Fl-GGA GUdC ACC C-Rh; H10/riboC, 5′-Fl-GGA GUC ACC C-Rh; SA11, 5′-Fl-GGA GUdC AGC CC-Rh; SA12, 5′-Fl-GGA GUdC AGG CCC-Rh; SA13, 5′-Fl-GGA GUdC AGG ACC C-Rh; SA13/riboC, 5′-Fl-GGA GUC AGG ACC C-Rh; SA13/Rh, GGA GUdC AGG ACC C-Rh; SA13/Fl, 5′-Fl-GGA GUdC AGG ACC C; SA14, 5′-Fl-GGA GUdC AGG AGC CC-Rh; SA15, 5′-Fl-GGA GUdC AGG AGA CCC-Rh; SA16, 5′-Fl-GGA GUdC AGG AGA GCC C-Rh; SA17, 5′-Fl-GGA GUdC AGG AGA GAC CC-Rh; RC18, 5′-Fl-GGA GGU CUG AUG AGG CCC-Rh.
16. Absorption spectra were taken on a Uvicon 820 (Kontron, Zürich) spectrophotometer. Steady-state fluorescence spectra were recorded under "magic angle" conditions on an SLM 8000S instrument (SLM Aminco, Urbana IL) corrected for lamp and wavelength fluctuations. Emission fluorescence spectra $F\lambda_{em},\lambda_{ex}$) for FRET analysis were collected over a broad range of emission wavelengths (λ_{ex} = 490 nm, λ_{em} = 500 to 650 nm; λ_{ex} = 560 nm, λ_{em} = 570–650 nm). Fluorescence anisotropies $r(\lambda_{em},\lambda_{ex})$ were determined from measurements of fluorescence intensities with vertical excitation polarizers with vertical ($F_{\parallel}$) and horizontal ($F_{\perp}$) emission polarizers according to $r = (F_{\parallel} - F_{\perp})/(F_{\parallel} + 2 \cdot F_{\perp})$. For fluorescence measurements, a solution of 350 nM of fluorescent duplex was adjusted to 2 μM of complementary unlabeled strand in 50 mM sodium cacodylate (pH 7.5), 10 mM $MgCl_2$. This condition is that for efficient single-turnover in ribozyme cleavage essays. The solutions were incubated for 3 min at 54°C and cooled slowly (within 2 to 3 hours) to 25°C, at which time the spectra were recorded.
17. The efficiency of dipole-dipole FRET from a donor D to an acceptor A is given by the Förster equation (*27*):

$$E = 1/1 + (R/R_0)^6 \quad (1)$$

    where R is the separation of the dyes and R_0 is the characteristic Förster distance. R_0^6 contains as factors an orientation parameter (κ^2) and the fluorescence quantum yield of the donor. For rapid randomization of the relative orientation between D and A, assumed in this study, κ^2 = 2/3 (*11, 27, 34*). The high anisotropy of 5-carboxytetramethylrhodamine, r(590,560) = 0.31, despite the low anisotropy of 5-carboxyfluorescein, r(520,490) = 0.13, indicates the need for a more critical evaluation of κ^2 in these systems (Fig. 3).
18. FRET efficiencies were determined from the sensitization of the acceptor fluoresence. The fluorescence intensities of the emission spectra $F(\lambda_{em},490)$ (excited at 490 nm where both 5-carboxytetramethylrho-

damine and 5-carboxyfluorescein absorb) were fit to the weighted sum of standard spectrum of a duplex labeled only with donor $F^D(\lambda_{em},490)$ and the fluorescence signal of the sample $F(\lambda_{em},560)$ excited at 560 nm (where only 5-carboxytetramethylrhodamine absorbs)

$$F(\lambda_{em},490) = c \cdot F^D(\lambda_{em},490) + (ratio)_A \cdot F(\lambda_{em},560) \quad (2)$$

c and $(ratio)_A$ are the fitted weighting factors of the two spectral components. The fit was made in the range λ_{em} = 500 to 540 nm (where only D emits) and λ_{em} = 570 to 650 nm (where both D and A emit). $(ratio)_A$ is the acceptor fluorescence signal of the FRET measurement normalized by $F(\lambda_{em},560)$ as shown in Eq. 4 (*34*).

$$(ratio)_A = \frac{F(\lambda_{em},490) - c \cdot F^D(\lambda_{em},490)}{F(\lambda_{em},560)} = E \cdot \frac{\varepsilon^D(490)}{\varepsilon^A(560)} + \frac{\varepsilon^A(490)}{\varepsilon^A(560)} \quad (3)$$

$(ratio)_A$ is linearly dependent on the efficiency of transfer E; it normalizes the sensitized FRET signal for the quantum yield of 5-carboxytetramethylrhodamine, for the concentration of the duplex molecule, and for any error in percentage of acceptor labeling. ε^D and ε^A are the molar absorption coefficient of D and A at the given wavelength. The ratio of absorption coefficient $\varepsilon^D(490)/\varepsilon^A(560)$ = 0.43 was determined from the absorbance spectra of the doubly labeled molecules and $\varepsilon^A(490)/\varepsilon^A(560)$ = 0.08 was determined from the excitation or absorbance spectrum of a singly 5-carboxytetramethylrhodamine-labeled molecule.

. S. Arnott, D. W. L. Hukins, S. D. Dover, *Biochem. Biophys. Res. Commun.* **48**, 1392 (1972).
. H. Goldstein, *Classical Mechanics* (Addison-Wesley, Reading, MA, ed. 2, 1980).
. Sequences of hammerhead riboxymes and substrates. S and R represent complementary sets of oligoribonucleotides where either R or S carries both of the dyes. See also reference for RNA duplexes (*15*).

Construct **A**: SA11, RA11, 5′-GGG CUC UGA UGA GCG CAA GCG AAA CUC C; SA12, RA12, 5′-GGG CCU CUG AUG AGC GCA AGC GAA ACU CC; SA13, RA13, 5′-GGG UCC UCU GAU GAG CGC AAG CGA AAC UCC; SA14, RA14, 5′-GGG CUC CUC UGA UGA GCG CAA GCG AAA CUC C; SA15, RA15, 5′-GGG UCU CCU CUG AUG AGC GCA AGC GAA ACU CC; SA16, RA16, 5′-GGG CUC UCC UCU GAU GAG CGC AAG CGA AAC UCC; SA17, RA17, 5′-GGG UCU CUC CUC UGA UGA GCG CAA GCG AAA CUC C. **B**: RB13, 5′-Fl-GGA CCG AAA CCC C-Rh, SB13, 5′-GGG GUdC AGG ACC GCA AGG UCC UCU GAU GAG GUC C; RB14, 5′-Fl-GGA CCG AAA CUC CC-Rh, SB14, 5′-GGG AGU dCAG GAC CGC AAG GUC CUC UGA UGA GGU CC; RB15, 5′-Fl-GGA CCG AAA CUG CCC-Rh, SB15, 5′-GGG CAG UdCA GGA CCG CAA GGU CCU CUG AUG AGG UCC; RB17, 5′-Fl-GGA CCG AAA CUG UGC CC-Rh, SB17, 5′-GGG CAC AGU dCAG GAC CGC AAG GUC CUC UGA UGA GGU CC. **C**: RC18, SC18, 5′-GGG CCG AAA CUG CCG CAA GGC AGU dCAC CUC C. **D**: RD20, 5′-Fl-GGA GCG UCU GAU GAG GGC CC-Rh, SD20, 5′-GGG CCC GAA ACU GCC GCA AGG CAG UdCA CGC UCC.

22. T. Tuschl and F. Eckstein, *Proc. Natl. Acad. Sci. U.S.A.* **90**, 6991 (1993).
23. H.-Y. Mei, T. W. Kaaret, T. C. Bruice, *Proc. Natl. Acad. Sci. U.S.A.* **86**, 9727 (1989).
24. F. U. Gast, K. M. A. Amiri, P. J. Hagerman, *Biochemistry* **33**, 1788 (1994).
25. E. Westhof, P. Dumas, D. Moras, *J. Mol. Biol.* **184**, 119 (1985).
26. K. J. Hertel *et al.*, *Nucleic Acids Res.* **20**, 3252 (1992).
27. T. Förster, *Fluoreszenz Organischer Verbindungen* (Vandenhoeck & Ruprecht, Göttingen, 1951); J. R. Lakowicz, *Principles of Fluorescence Spectroscopy* (Plenum Press, New York, 1983).
28. C. Massire, C. Gaspin, E. Westhof, *J. Mol. Graphics* **12**, 201 (1994).
29. T. Tuschl, M. M. P. Ng, W. Pieken, Benseler, F. Eckstein, *Biochemistry* **32**, 11658 (1993).
30. P. Theisen *et al.*, *Tetrahedron Lett.* **33**, 5033 (1992).
31. H. Aurup, T. Tuschl, F. Benseler, J. Ludwig, F. Eckstein, *Nucleic Acids Res.* **22**, 20–24 (1994).
32. K. J. Hertel, D. Herschlag, O. C. Uhlenbeck, *Biochemistry* **33**, 3374 (1994).
33. A. C. Jeffries, R. H. Symons, *Nucleic Acids Res.* **17**, 1371 (1989).
34. R. N. Clegg, *Methods Enzymol.* **211**, 353 (1992).

35. We thank R. Clegg and G. Vámosi, Göttingen, for discussions and advice, U. Kutzke, G. Heim, and A. Zechel, Göttingen, for technical assistance, A. Heaton, B. Patel, and C. S. Vörtler, Göttingen, for critical reading of the manuscript. Supported by the Deutsche Forschungsgemeinschaft and the Fonds der Chemischen Industrie (F.E.) and an EEC grant (E.W.). Coordinates of the P atoms have been deposited at the Brookhaven Protein Data Bank.

9 August 1994; accepted 11 October 1994

Isolation of the Tomato *Cf-9* Gene for Resistance to *Cladosporium fulvum* by Transposon Tagging

David A. Jones, Colwyn M. Thomas, Kim E. Hammond-Kosack, Peter J. Balint-Kurti,* Jonathan D. G. Jones†

Sainsbury Laboratory, John Innes Centre, Norwich Research Park, Colney Lane, Norwich, NR4 7UH, UK.

*Present address: Laboratory of Cellular and Developmental Biology, National Institute of Diabetes and Digestive and Kidney Diseases, National Institutes of Health, Bethesda, MD 20892, USA.

†To whom correspondence should be addressed.

The tomato *Cf-9* gene confers resistance to infection by races of the fungus *Cladosporium fulvum* that carry the avirulence gene *Avr9*. The *Cf-9* gene was isolated by transposon tagging with the maize transposable element *Dissociation*. The DNA sequence of *Cf-9* encodes a putative membrane-anchored extracytoplasmic glycoprotein. The predicted protein shows homology to the receptor domain of several receptor-like protein kinases in *Arabidopsis*, to antifungal polygalacturonase-inhibiting proteins in plants, and to other members of the leucine-rich repeat family of proteins. This structure is consistent with that of a receptor that could bind Avr9 peptide and activate plant defense.

Plants can defend themselves against infection by viruses, bacteria, fungi, nematodes, insects, and even other plants. Plant defenses are often activated by specific interaction between the product of a disease resistance (*R*) gene in the plant and the product of a corresponding avirulence (*Avr*) gene in the pathogen (*1*). Without either of these genes, plant defenses are not activated and infection by the pathogen is permitted. To understand how specific plant defense is regulated, it is necessary to learn the nature of the *R* and *Avr* gene products, the way they interact, and the chain of events that results.

In the interaction between tomato (*Lycopersicon esculentum*) and the leaf mould fungus *Cladosporium fulvum*, the avirulence gene *Avr9* has been characterized (*2*). *Avr9* specifies a 28–amino acid secreted peptide that elicits a necrotic response when injected into tomato plants carrying the *Cf-9* resistance gene. We have now isolated *Cf-9* by transposon tagging, using a maize *Activator-Dissociation* element (*Ac-Ds*)–based system to target a specific gene from tomato. To tag *Cf-9*, we used a transgenic tomato line (*3*) carrying a *Ds* element located 3 centimorgans (*4*) from the *Cf-9* locus, which had previously been mapped to the short arm of chromosome 1 (*5*). To activate this *Ds* element, we used a genetically unlinked stabilized *Ac* (*sAc*), itself incapable of transposition (*6*). Appropriate crosses and selections were carried out (Fig. 1A) to produce plants heterozygous for *Ds* and *sAc* and homozygous for *Cf-9*. These plants were crossed to plants lacking *Cf-9* but homozygous for an *Avr9* transgene (*7*, *8*) (Fig. 1A). The progeny of this cross, which were heterozygous for *Cf-9* and *Avr9*, became necrotic and died shortly after seed germination, but those mutant for *Cf-9* survived (Fig. 1B).

Approximately 160,000 progeny were germinated (Fig. 1B) and 118 survivors were recovered. Of these, 65 arose by clonal propagation of 10 independent mutations (*8*). The remaining 53 arose independently, giving a total of 63 independent mutations. Of these, 21 were variegated for necrosis (Fig. 1C) and carried both *Ds* and *sAc*, 33 were stable and carried *Ds*, and 9 were stable but did not carry *Ds*. In addition to the 21 variegated mutations that were inferred to carry *Ds* insertions in *Cf-9*, 16 more were identified among the stable mutants by activation with *sAc*, which suggests a total of at least 37 independent *Ds* inser-